

# Real-time dynamics of single-electron pumpings

Chuan-Yu Lin<sup>1</sup> and Wei-Min Zhang<sup>1,\*</sup>

<sup>1</sup>*Department of Physics and Center for Quantum information Science,  
National Cheng Kung University, Tainan 70101, Taiwan*

(Dated: June 20, 2012)

In this Letter, we study the real-time dynamics of single-electron pumpings. We modulate the left tunneling barrier along with the dot level but slightly changing the right barrier to operate the single-electron pumping device at zero bias. We show the adiabatic to the non-adiabatic transition in pumping operations. We also find that the relation  $I = e\omega/2\pi$  is only valid in the low operating frequency adiabatic regime.

PACS numbers: 85.35.Gv, 73.63.-b, 03.65.Yz

Charge pumps and turnstiles are nano-fabrication devices utilizing controllable external gate voltages to manipulate electron transfer. These devices are supposed to have important applications in quantum metrology and solid-state quantum computation. Charge pumping operations have been experimentally demonstrated with various double resonance tunneling structures, in particular, through two phase-shifted tunneling barriers[1–5] at the zero and non-zero bias voltages. These experiments are aiming at the goals of a high current at high frequency with high accuracy of the pumps[5, 6], in order to meet the standard quantum metrology error rate ( $< 10^{-7}$ ). As a subsequent work of Ref. [7], we study in this letter the single-electron pumping by modulating time-dependent tunneling barriers along with the energy level of the dot through the external gate voltages at zero-bias.

By modulating the tunnel barriers and the dot level, it has been observed[1–5] that electrons can be transferred one-by-one between the source and the drain. In our previous work[7], we have studied the time-dependent single-electron dynamics by modulating the left and right tunneling barriers in anti-phase but fixing the dot level, with a finite bias voltage, to examine the high frequency limit of pumping operations. Here we shall follow the experimental setup given in Ref. [2, 3, 5] for a different operating mode, namely modulating the left tunneling barrier along with the dot level but fixing or slightly changing the right barrier, and operate the device at zero bias. We should study both the adiabatic and non-adiabatic pumpings through different operating frequencies.

Utilizing the recently developed non-equilibrium quantum transport theory[8] which is derived from the exact master equation for nanoelectronics[9], we obtain the time-dependent electron occupation in the dot and the time-dependent electron current flowing from each lead

into the dot:

$$n(t) = v(t, t) + u(t, t_0)n(t_0)u^\dagger(t, t_0), \quad (1a)$$

$$I_\alpha(t) = -\frac{2e}{\hbar} \text{Re} \int_{t_0}^t d\tau \text{Tr} \left\{ g_\alpha(t, \tau) v(\tau, t) - \tilde{g}_\alpha(t, \tau) \times u^\dagger(t, \tau) + g_\alpha(t, \tau) u(\tau, t_0) n(t_0) u^\dagger(t, t_0) \right\}. \quad (1b)$$

Here  $\alpha = L, R$  denote the left and right leads (the source and the drain), and  $n(t_0)$  is the initial electron occupation in the dot. The function  $u(\tau, t_0)$  and  $v(\tau, t)$  are the two-point Green functions that satisfies the Dyson equation[8, 9], and the non-local time-correlation function is given by  $g_\alpha(\tau, \tau') = \int \frac{d\omega}{2\pi} J_\alpha(\omega, \tau, \tau') e^{-i\omega(\tau-\tau')}$  and  $\tilde{g}_\alpha(\tau, \tau') = \int \frac{d\omega}{2\pi} J_\alpha(\omega, \tau, \tau') f_\alpha(\omega) e^{-i\omega(\tau-\tau')}$  with  $g(\tau, \tau') = g_L(\tau, \tau') + g_R(\tau, \tau')$  and  $\tilde{g}(\tau, \tau') = \tilde{g}_L(\tau, \tau') + \tilde{g}_R(\tau, \tau')$ , where  $f_\alpha(\omega) = \frac{1}{e^{\beta(\omega-\mu_\alpha)} + 1}$  is the initial electron distribution function of lead  $\alpha$  at the inverse initial temperature  $\beta = 1/k_B T$ , and  $\mu_\alpha$  the corresponding chemical potential. The spectral density  $J_\alpha(\omega, \tau, \tau') = 2\pi \varrho_\alpha(\omega) V_\alpha(\tau) V_\alpha^*(\tau')$ , where  $\varrho_\alpha(\omega)$  is the density of states of the lead and  $V_\alpha(\tau)$  the lead-dot coupling coefficient. The integrate kernels  $g(\tau, \tau')$  and  $\tilde{g}(\tau, \tau')$  take into account all the non-Markovian back-reaction memory effects from the leads (reservoirs) associating with quantum dissipation and fluctuation.

Similar to the previous work[7], we take the spectral densities with a Lorentzian-type shape,

$$J_\alpha(\omega, \tau, \tau') = \frac{V_\alpha(\tau) V_\alpha^*(\tau') W_\alpha^2}{(\omega - \mu_\alpha)^2 + W_\alpha^2}, \quad (2)$$

where  $V_\alpha(\tau)$  are the time-dependent electron tunneling amplitude between lead  $\alpha$  and the dot that can be controlled by the gate voltage  $V_{G\alpha}(t)$ , and  $W_\alpha$  is the bandwidth of the spectral density. The explicit relation between the tunneling rate and the gate voltage can be obtained by solving the Schrödinger equation for a one-dimensional scattering problem. Here we obtain

$$V_\alpha(t) \simeq \frac{2}{\sqrt{A(t) \cosh^2(2k_\alpha(t)a) + B(t) \sinh(2k_\alpha(t)a)}}, \quad (3)$$

\*Electronic address: wzhang@mail.ncku.edu.tw

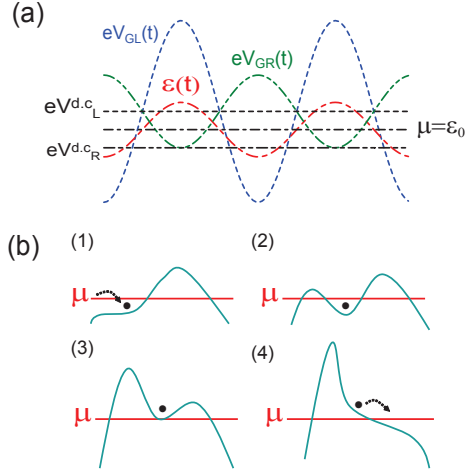


FIG. 1: (color online) (a) The driving fields on the left gate (blue dot line), the right gate (green dash-dot-dot line), and the dot level (red dash-dot line):  $V_{GL}(t) = V_L^{dc} - V_L^{ac} \cos(\omega_c t)$ ,  $V_{GR}(t) = V_R^{dc} + V_R^{ac} \cos(\omega_c t)$ , and  $\varepsilon(t) = \varepsilon_0 - \varepsilon_c \cos(\omega_c t)$ . (b) Schematic plots of the barriers changing at four different times in each cycle.

where  $A(t) = (1 + \frac{k_2}{k_1})^2$  and  $B(t) = (\frac{k_1 k_2 - k_\alpha^2}{k_1 k_\alpha})$  with  $k_\alpha(t) = \sqrt{\frac{2m^*(eV_{G\alpha}(t) - \mu)}{\hbar^2}}$ ,  $k_1 = \sqrt{\frac{2m^*\mu}{\hbar^2}}$  and  $k_2 = \sqrt{\frac{2m^*\varepsilon(t)}{\hbar^2}}$ , where  $a$  is the width of the barriers, and  $m^*$  is the effective mass of the electron in the sample. We apply different sinusoidal wave modulation to the tunneling barriers and the dot level:  $V_{G\alpha}(t) = V_\alpha^{dc} - V_\alpha^{ac} \cos(\omega_c t)$ ,  $\varepsilon(t) = \varepsilon_0 - \varepsilon_c \cos(\omega_c t)$ . It shows that the tunneling rate between lead  $\alpha$  and the dot is determined not only by the gate voltage  $V_\alpha(t)$  acting on the barrier between them but also the gate voltage  $\varepsilon(t)$  acting on the dot level.

Figure 1(a) shows the corresponding driven fields:  $V_{GL}(t)$ ,  $V_{GR}(t)$ , and  $\varepsilon(t)$ , and their relative phase.  $V_\alpha^{dc}$  and  $V_\alpha^{ac}$  are the external d.c and a.c field applied on the barrier,  $\varepsilon_0$  is the energy of the dot level, and  $\varepsilon_c$  is the oscillation amplitude of the ac gate field applied on the dot. Fig. 1(b) show a schematic barrier modulating process. In the first half of the pumping operation, (1)-(2), the left barrier is opened to the source and the right barrier is closed. The electron tunnel from the source to the dot. In the second half of the cycle, (3)-(4), the electrons transfers from the dot to the drain because the left barrier is closed and the right barrier is opened.

Now, we analyze how the electron turnstile operates with time-dependent tunneling barriers along with the dot level at zero bias. To be specific, we fix the bandwidth of the spectral density by  $W_{L,R} = 2$  meV, and the initial temperature of the leads at  $k_B T = 0.01$  meV, i.e.  $T \simeq 116$  mK. We begin with an equal dc voltage on both the left and the right barriers,  $eV_L^{dc} = eV_R^{dc} = 1.6$  meV. Fig. 2 shows the time-dependent electron population in the dot, the left and the right currents flowing into the dot as well as the pumping current  $I(t) = \frac{1}{2}[I_L(t) - I_R(t)]$  with a sinusoidal wave gate voltage modulating the left

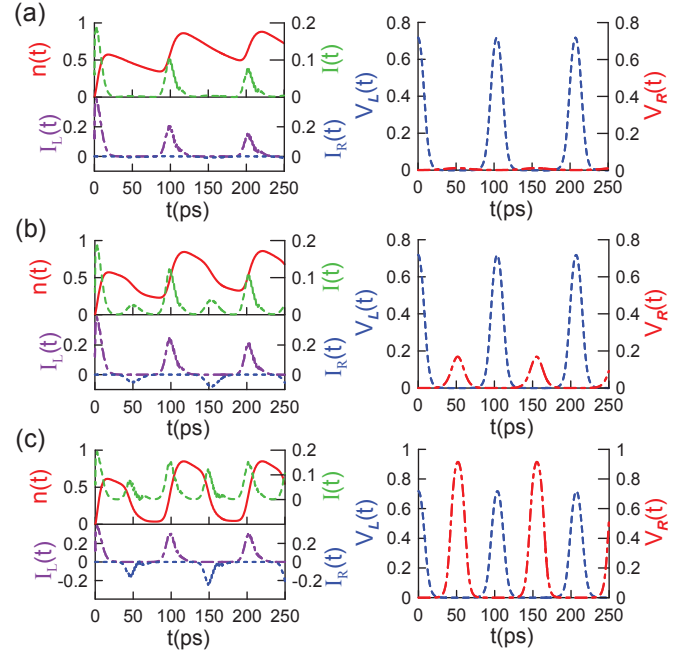


FIG. 2: (color online) The left column shows the time-dependent electron occupation (the red solid line), the pumping current (the green dash-dash line), left current (purple dash-dot line) and right current (blue dotted-dotted line) altered by the sinusoidal wave modulation on the left tunneling barrier with  $eV_L^{dc} = 1.6$  meV and  $eV_L^{ac} = 0.8$  meV, along with the dot level with  $\varepsilon_c = 0.2$  meV, but the right barrier with  $eV_R^{dc} = 1.6$  meV and (a)  $eV_R^{ac} = 0$ , (b)  $eV_R^{ac} = 0.4$  meV, and (c)  $eV_R^{ac} = 0.8$  meV. The driving field frequency  $\omega_c = 10$  GHz. The right column shows the corresponding time-dependent tunneling amplitude of the left and right barriers. The initial temperature of the source and drain is set at  $kT \simeq 116$  mK.

tunneling barriers along with the dot level. The ac field strength on the left barrier and the dot level are given by  $eV_L^{ac} = 0.8$  meV and  $\varepsilon_c = 0.2$  meV. All these parameters are adjustable in experiments. We find that with zero ac field on the right barrier, the tunneling amplitude for electrons transiting from the dot to the drain is almost zero [see the right plot of Fig. 2(a)] to make electrons tunnel through the device. i.e.  $I_R(t) \simeq 0$  as shown in the left plot of Fig. 2(a). Increasing  $eV_R^{ac} = 0.4$  meV, the corresponding tunneling amplitude is still not large enough to make the single-electron pumping, see Fig. 2(b). Only when the ac field strength is increased upon  $eV_R^{ac} = 0.8$  meV, electrons can transit one by one, see Fig. 2(c).

To make single-electron pumping operations with a fixed or small modulated right barrier, we may check the dc voltage effect on the right barrier under a small ac field along with the dot level, e.g.  $V_R^{ac} = \varepsilon_c = 0.2$  meV. Figures 3(a) to (c) show that a smaller dc field acting on the right barrier can increase the amplitude of the electron occupation oscillation. However, the overlap of the left and right currents (see Fig. 3(c)) indicates that electrons also flow back from the drain to the dot in the

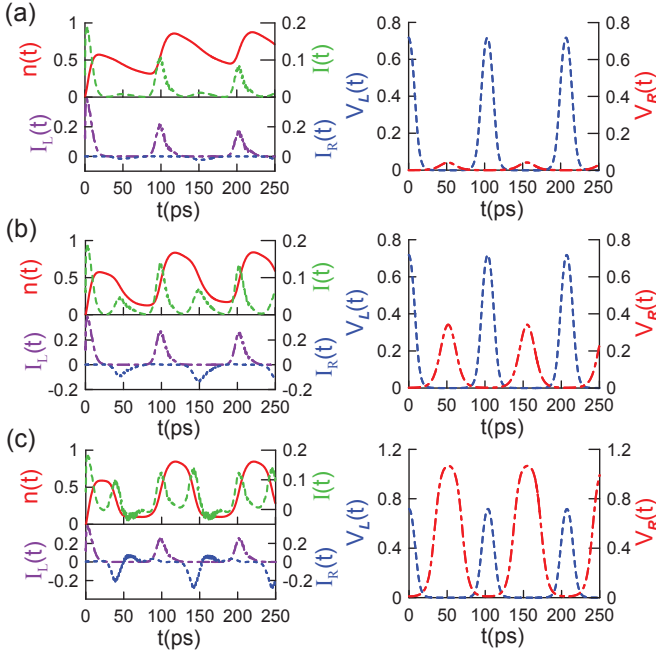


FIG. 3: (color online) The same plots as Fig. 2 with different setup. Here the ac field  $eV_R^{ac} = 0.2$  meV is fixed but the dc field is changed to (a)  $eV_R^{dc} = 1.6$  meV, (b)  $eV_R^{dc} = 1.3$  meV, and (c)  $eV_R^{dc} = 1.0$  meV. The other parameters are the same as in Fig. 2.

second half of the pumping cycle (as a leakage effect). In other words, reducing the dc field on the right barrier messes up the electrons pumping direction.

The remaining controllability is the ac field on the dot level. We take  $V_R^{dc} = 1.4$  meV so that the leakage effect is negligible, and keep the ac field on the right barrier relatively small,  $eV_R^{ac} = 0.2$  meV, compared to  $eV_R^{ac} = 0.8$  meV. Figures 4 shows the result of electron transition with different ac field acting on the dot level. For a small ac field,  $\varepsilon_c = 0.1$  meV, electrons cannot tunnel through the dot one by one because of the small tunneling amplitude, see Fig. 4(a). Increasing  $\varepsilon_c$  ( $= 0.3$  meV in Fig. 4(b)) makes the tunneling amplitude larger, but not larger enough to reach the single-electron pumping. When  $\varepsilon_c$  is increased to 0.5 meV, the electron can tunnel through the dot one by one, as shown in Fig. 4(c).

Putting all the above results together shows that a good single-electron pumping operation, by modulating the left tunneling barrier along with the dot level but fixing or slightly changing the right barrier at zero bias, requires (i) a high dc field on the left barrier with a slightly low dc field on the right barrier to avoid electrons from leakage; and (ii) a large overlapping area between  $\varepsilon(t)$  and  $eV_{GR}(t)$  to ensure electrons transferring through the dot one by one. A relatively large  $\varepsilon(t)$  can actually induce a large tunneling amplitude between the dot and the right lead because of the off-phase with the small ac field on the right barrier. Thus the mechanism for

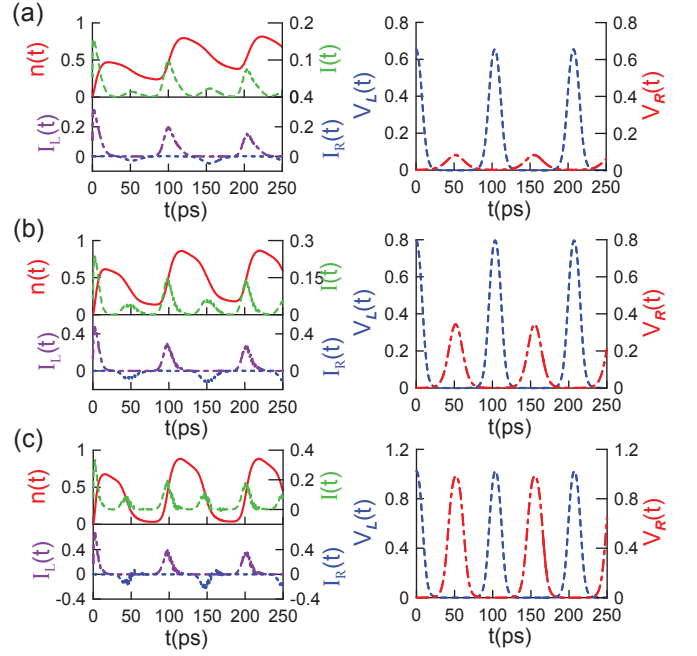


FIG. 4: (color online) The same plots as Fig. 2 with fixing  $eV_R^{dc} = 1.4$  meV and  $eV_R^{ac} = 0.2$  meV but changing the ac field on the dot level with (a)  $\varepsilon_c = 0.1$  meV, (b)  $\varepsilon_c = 0.3$  meV, and (c)  $\varepsilon_c = 0.5$  meV. The other parameters are the same as in Fig. 2

single-electron pumping operations by modulating the left tunneling barrier along with the dot level but fixing or slightly changing the right barrier at zero bias is indeed equivalent to the single-electron pumping through modulating the left and right tunneling barriers in anti-phase but fixing the dot level at a finite bias[7].

Next we examine the single-electron pumping with different operation frequencies. As we have shown[7], there is a character time, i.e. the dwell time or dwell frequency  $\omega_d$ . When the modulation frequency is smaller than the dwell frequency  $\omega_c < \omega_d$ , the electron have enough time to tunnel into the dot. Therefore, the electron have the higher probability to be adiabatically transited one by one in each cycle. In the high frequency regime,  $\omega_c > \omega_d$ , on the contrary, only an electron can partially tunnel from the source to the drain (a non-adiabatic process). Figure 5(a) shows the transition from adiabatic to non-adiabatic regime for the electron occupation in the dot. In the adiabatic regime, the variation of the electron occupation is almost one because the pumping period is much longer than the intrinsic time scale of the system. However, When the modulation frequency locates in the non-adiabatic regime, the electron cannot have enough time to response to the external driving field so that the electron occupation in the dot varies fractionally. Moreover, Fig. 5(b) gives the average current with respect to the driving frequency. It shows that for  $\omega_c < \omega_d/2$ , the pumping current has a linear relation with the modu-

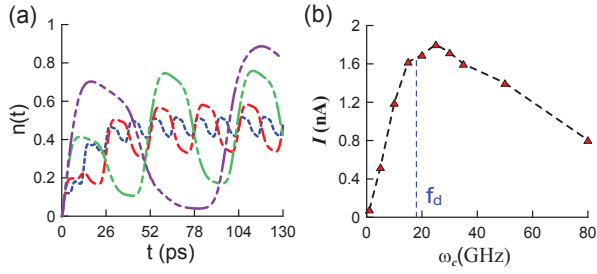


FIG. 5: The adiabatic to the non-adiabatic transition via the modulation frequency. (a) The electron occupation in the dot with  $f_{sin} = 10$  GHz (purple dash-dotted-dotted line), 20 GHz (green dash-dotted-dotted line), 40 GHz (red dash-dotted line), and 80 GHz (blue dash line). (b) The pumping current as a function of the modulation frequency. Other parameters are the same in Fig. 4(c).

lation frequency,  $I = e\omega/2\pi$ . When the operating frequency  $\omega_c > \omega_d/2$ , the frequency dependence of the transport current deviates from the linear regime substantially. A similar result is obtained in Ref. [10] recently.

In conclusion, the analysis based on the real-time electron transport shows that the dc field strength, the amplitude of driving ac field and the modulation frequency make the single-electron pumping device behave significantly different. The larger overlapping area between  $\varepsilon(t)$  and  $V_{GR}(t)$ , and the relatively lower operating frequency are the two requirements for increasing the accuracy of single-electron pumpings and making the device a good candidate for metrological applications.

This work is supported by the National Science Council of ROC under Contract No. NSC-99-2112-M-006-008-MY3 and National Center for Theoretical Science.

- 
- [1] L. P. Kouwenhoven, A. T. Johnson, N. C. van der Vaart, C. J. P. M. Harmans, and C. T. Foxon, *Phys. Rev. Lett.* **67**, 1626 (1991).
  - [2] A. Fujiwara, N. M. Zimmerman, Y. Ono, and Y. Takahashi, *Appl. Phys. Lett.* **84**, 1323 (2004); A. Fujiwara, K. Nishiguchi and Y. Ono, *Appl. Phys. Lett.* **92**, 042102 (2008).
  - [3] M. D. Blumenthal, B. Kaestner, L. Li, S. Giblin, T. J. B. M. Janssen, M. Pepper, D. Anderson, G. Jones and D. A. Ritchie, *Nat. Phys.* **3**, 343 (2007).
  - [4] J. P. Pekola, J. J. Vartiainen, M. Möttönen, O.-P. Saira, M. Meschke, and D. V. Averin, *Nat. Phys.* **4**, 120 (2008).
  - [5] S. P. Giblin, S. J. Wright, J. D. Fletcher, M. Kataoka, M. Pepper, T. J. B. M. Janssen, D. A. Ritchie, C. A. Nicoll, D. Anderson, and G. A. C. Jones, *New J. Phys.* **12**, 073013 (2010).
  - [6] S. J. Wright, M. D. Blumenthal, M. Pepper, D. Anderson, G. A. C. Jones, C. A. Nicoll, and D. A. Ritchie, *Phys. Rev. B* **80**, 113303 (2009).
  - [7] C. Y. Lin and W. M. Zhang, *Appl. Phys. Lett.* **99**, 072105 (2011), in which a mistake in the formula of spectral density is corrected here.
  - [8] J. S. Jin, M. W. Y. Tu, W. M. Zhang, Y. J. Yan, *New J. Phys.* **12**, 083013 (2010).
  - [9] M. W. Y. Tu and W. M. Zhang, *Phys. Rev. B* **78**, 235311 (2008).
  - [10] F. Pellegrini, C. Negri, F. Pistolesi, N. Manini, G. E. Santoro, and E. Tosatti, *Phys. Rev. Lett.* **107**, 060401 (2011).